Supporting Information for

Access to Aliphatic Protons as Reporters in Non-Deuterated Proteins by Solid-State NMR

Suresh Kumar Vasa[a], Petra Rovó[a], Karin Giller[a], Stefan Becker[a], and Rasmus Linser[a*]

[a]Department of NMR-based Structural Biology, Max Planck Institute for Biophysical Chemistry, 37077 Göttingen, Germany

Experimental Details:

Preparation of uniformly [^{13}C, ^{15}N]-labeled SH3:
Uniformly ^{13}C-, ^{15}N- label SH3 domain of chicken α-spectrin protein was prepared using procedures as described earlier[1]. Since heating is uncritical for the pulse sequences involved, we added 75 mM of $(NH_4)_2[Cu(edta)]$ to speed up the NMR measurements. The addition of paramagnetic ions decreased the spin-lattice relaxation (^{1}H-T_1 is around 150 ms) without compromising the resolution of the spectra. The resulting pellet was packed into a 1.3 mm rotor.

Solid-state NMR spectroscopy and analysis.
All solid-state NMR experiments were acquired using an 800 MHz AVANCE-II spectrometer supplied with a 1.3 mm HCN Bruker probe. The MAS spinning speed was set to 55.555 kHz for the measurements. (The spinning stability was around ± 50 Hz.) The real temperature of the sample was around 35 °C. Temperature calibration was done using a KBr sample by calibrating the temperature dependence of ^{79}Br chemical shift under similar experimental conditions. The pulse sequence for time-shared ^{1}H-^{13}C/^{15}N-^{1}H-correlation experiment is shown in Figure S3. An eight step phase cycling (two-step each for Φ_1, Φ_1, and Φ_3) was done to suppress direct magnetization signal. 90° pulses of 5.5 μs (45.45 kHz), 5.2 μs (48 kHz) and 6.8 μs (36.8 kHz) were used on ^{1}H, ^{13}C, and ^{15}N channels, respectively. Water suppression was achieved using the MISSISSIPPI strategy[2] (12 kHz and 80 ms duration) and J-decoupling using WALTZ-64 with 2.5 kHz of proton rf field strength during acquisition. For iSOCP transfer, an RF field strength of 15 kHz was used on both channels. For DQCP, an rf field strength of 9.6 kHz on the proton channel (square pulse) and 51 kHz on ^{15}N/^{13}C channel (using a tangential shape) was applied. The proton offset was set to the water frequency throughout the experiment. Each 2D proton-proton correlation (Figure S6) was recorded in one hour with 72 scans and an inter-scan delay of 0.2 seconds. The indirect proton dimension had a total acquisition time of 8 ms (250 t_1 points). The 3D ^{1}H-^{13}C/^{15}N-^{1}H time-shared experiment (Figure 3) was recorded in 34 hours with 8 scans for each time increment and an inter-scan delay of 0.2 seconds. A total of 100 t_1 and 260 t_2 increments were used resulting in a total acquisition time of 5 ms for ^{1}H (t_1), 7.4 ms, for ^{13}C (t_2) and 12.3 ms for ^{15}N in the indirect dimensions. All the indirect dimensions were acquired either using TPPI or STATES-TPPI phase-sensitive incrementation. All processing of the experimental NMR spectra was done by TOPSPIN 3.2 software. For apodization, a sine-square function with an SSB factor of 4 was used in both direct and indirect dimensions of 3D-time-shared iSOCP spectrum. Base line correction and linear prediction was not applied for the processing of the spectrum.
A 3D-HNhH-RFDR experiment[3] was recorded in 30 hours using 8 scans for each increment with a relaxation delay of 0.3 seconds and a (RFDR) mixing duration of 1.72 ms. A total of 200 t_1 and 160 t_2 increments, resulting in total acquisition times of 17.6 ms and 8 ms in ^{15}N and ^{1}H indirect dimensions, respectively, were recorded. The RFDR pulse length was set to 8.88 μs with an rf field strength of 87.7 kHz. Similar processing for parameters as time-shared iSOCP spectrum (as described above) was used for processing the 3D spectrum.
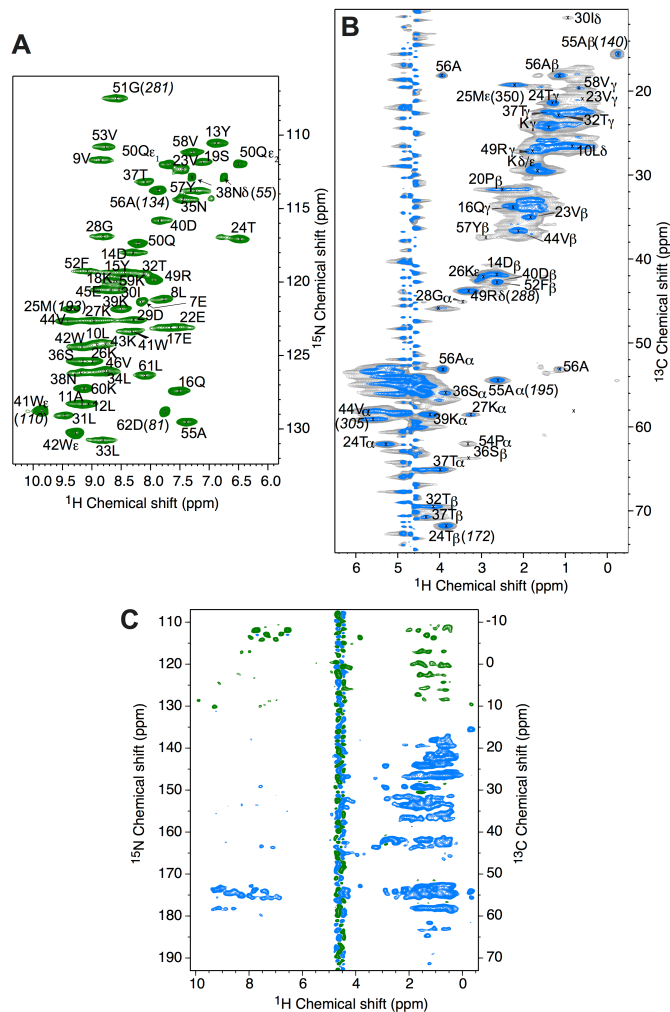
Figure S1. (A) ^{1}H-^{15}N and (B) ^{1}H-^{13}C correlation spectra of the SH3 domain of α-spectrin at a spinning speed of 56 kHz and 800 MHz proton Larmor frequency. The ridge in the HC spectrum is due to residual water signal after water suppression. The HC spectrum is shown with higher (in blue) and lower contour levels (in gray). For some resolved peaks, the observed proton linewidths (in Hz, values without apodization) are shown in parenthesis. (C) ^{1}H (direct dimension) -^{13}C/^{15}N (sum) projection plane of the time-shared 3D experiment whose strips are shown in Figure 2 of the main text. ^{15}N-edited (positive) peaks are shown in green color, whereas ^{13}C-edited (negative) peaks are shown in sky-blue color. All the experimental and processing parameters are similar as described in in Figure 2.
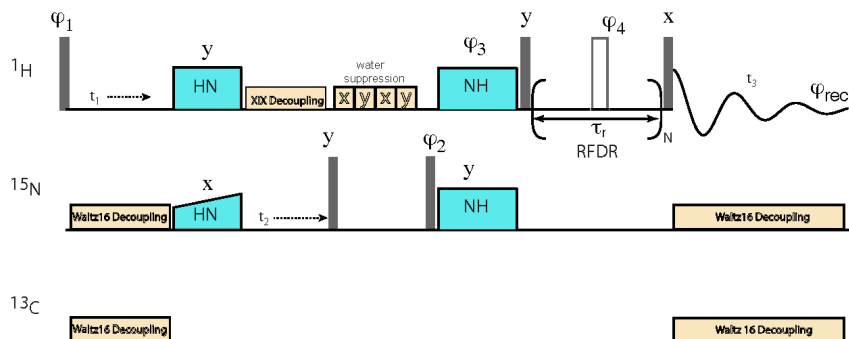
Figure S2. Pulse sequence used for recording the 3D HNhH correlation experiment. Proton-proton homonuclear magnetization transfer is achieved using RFDR mixing. Two-step phase cycles were employed for ϕ$_1$, ϕ$_2$, and ϕ$_3$ upon according inversion of the receiver phase. For (RFDR) 180° pulse phase ϕ$_4$, XY-16 phase cycling was employed.
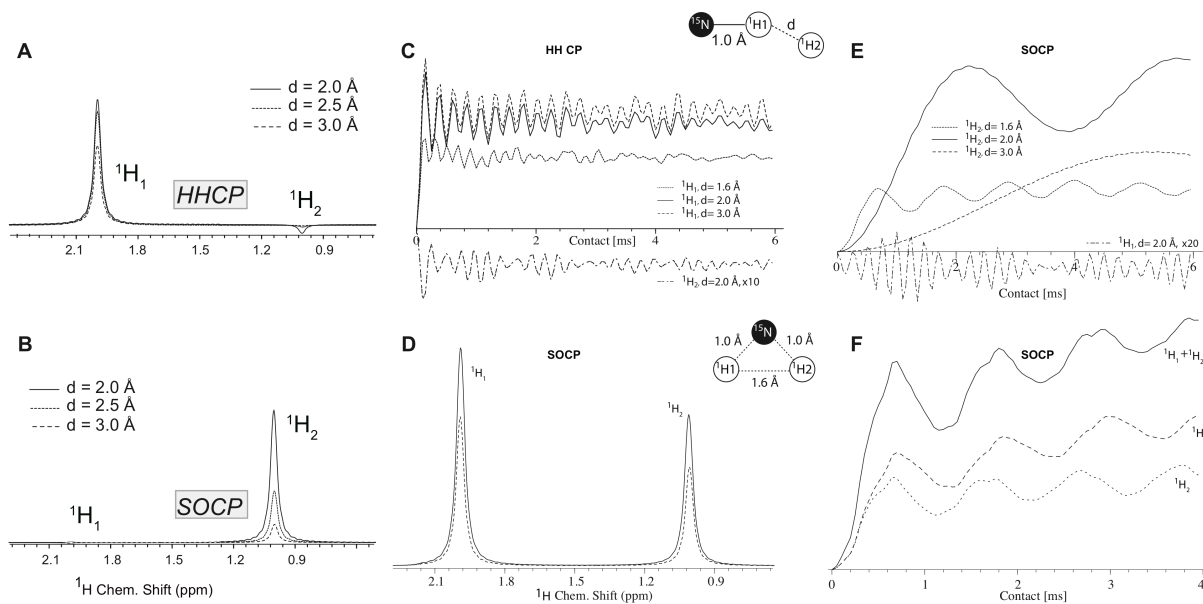
Figure S3. Numerical (SIMPSON) simulations of transfer pathways of the cross-polarization processes Hartmann-Hahn CP (A) and iSOCP (B). Here, transfer of magnetization from ^{15}N to proton spins was considered for a three-spin system including an amide nitrogen and amide proton coupled to a relayed proton with different distances. For the spin system depicted (top), the buildup curves of proton magnetization from initial nitrogen magnetization for (C) Double Quantum Hartmann-Hahn CP and (E) iSOCP are shown. The buildup curve for $^1H_2$ spin is scaled by 10 times and for $^1H_1$ spin is scaled by 20 times for visual clarity in (C) and (E), respectively. (D) and (F) show simulation curves for an NH_2 spin system as in sidechain amides. Simulated proton spectra with iSOCP transfer time of 1.5 ms (D) and buildup curves (F) are shown for both protons. In these simulations, 10 kHz of RF field strength for iSOCP transfer is assumed on both channels. In these simulations, the carrier was set to 0 ppm. See Figure S4 for dependencies on the carrier frequency during iSOCP. The vertical scale of FID signals in C, E, and F are intensity values in arbitrary units.

SIMPSON Simulations.

To analyse the iSOCP transfer process, SIMPSON simulations (see the input file below) for a three-spin (two protons and one nitrogen spin) system (as drawn in Main Text Figure 2A) were pursued. E. g., we considered a coupled ^{15}N^{1}H$_1$ (amide group) spin pair where $^1H_1$ is dipolar coupled to another proton spin ("relayed proton" $^1H_2$). Here we show the polarization transfer from ^{15}N to ^{1}H spins. Supplementary Figure 3B suggests that, for different strengths of proton-proton coupling and under iSOCP conditions, we obtain transfer of magnetization from the ^{15}N spin mostly to $^1H_2$ instead of the directly bonded $^1H_1$ spin, which is in contrast to the conventional Hartmann-Hahn (HH) CP (depicted in Supplementary Figure 3A). Importantly, for a distance of around 2 Å, maximum magnetization transfer is observed between amide nitrogen and relayed proton, using a mixing time of 1 to 2 milliseconds. For SIMPSON[4] simulations, a crystal file ("rep256") with 256 different orientations given by the "REPULSION" algorithm and ten gamma angles were used for imitating the powder averaging. A spinning speed of 55.55 kHz and a proton frequency of 800 MHz, similar to the experimental conditions, were considered for the simulations. All other couplings other than dipolar couplings were ignored here. For these simulations, a 10 kHz RF field strength was assumed during iSOCP. To differentiate between the two protons, slightly different chemical shifts (2 ppm for H_1 and 1 ppm for H_2) were used for the simulations, however, both close to on-resonance conditions. The carrier in the simulations on this system was initially assumed to be at 0 ppm on the proton channel and on-resonance on the nitrogen. An additional iSOCP simulation for an NH_2 (Figure S3D and S3F) spin system shows that here the polarization transfer is distributed almost equally between two protons due to proton-proton couplings. For the HHCP simulations, we used similar rf filed strengths as the experimental ones (see the experimental section above).

The effect of varying offsets on the iSOCP performance for the first system is assessed in Supplementary Figure 4. Compared to conventional HHCP, the iSOCP condition is relatively narrow in the simulation cases, thus its performance is sensitive to the offset chosen (Figure S4).

3

```
#Simpson Input file for simulations
spinsys {
channels  1H 15N
nuclei    1H 1H 15N
shift    1  2p  0 0 0 0 0
shift    2  1p  0 0 0 0 0
shift    3  0p  0 0 0 0 0
dipole  1 3 12180  0 0 0
#for 2 angstrom #
#dipole   1 2 -15015  0 0 0
#for 1.6 angstrom #
#dipole   1 2 -29326  0 0 0
#for 3.0 angstrom #
 dipole  1 2 -4449  0 0 0
}
par {
gamma_angles    10
spin_rate       55555
sw              25000
crystal_file    rep256
np              1024
start_operator  I3x
detect_operator I1p+I2p
method          direct
proton_frequency 800e6
verbose         1101
}
proc pulseq {} {

global par
set   ct    3000
set   rf_H   15000
set   rf_C   15000
set   dw    [expr 1e6/$par(sw)]
set   dipole1 [dist2dip 15N 1H 1.0]
set   dipole2 [dist2dip 1H 1H 3.0]
puts  "$dipole1; $dipole2"

reset
offset $par(off1)  0
pulse $ct  $rf_H 0 $rf_C 0
offset 0      0
acq

for {set j 1} {$j < $par(np) }  {incr j} {
delay  $dw
acq
        }
}
proc main {} {

global  par
set   par(outr)    [open "results.log" w]
for {set k 1} {$k < 21} {incr k} {
set   par(off1)   [expr -5000+(($k-1)*500)]
puts  $par(outr) "$k  $par(off1)\n"

set   f   [fsimpson]
fsave   $f  $par(name)_$par(off1).fid
fzerofill $f  8192
faddlb   $f  40 0
fft      $f
fsave    $f $par(name)_$par(off1).spe
funload  $f
}
}
```
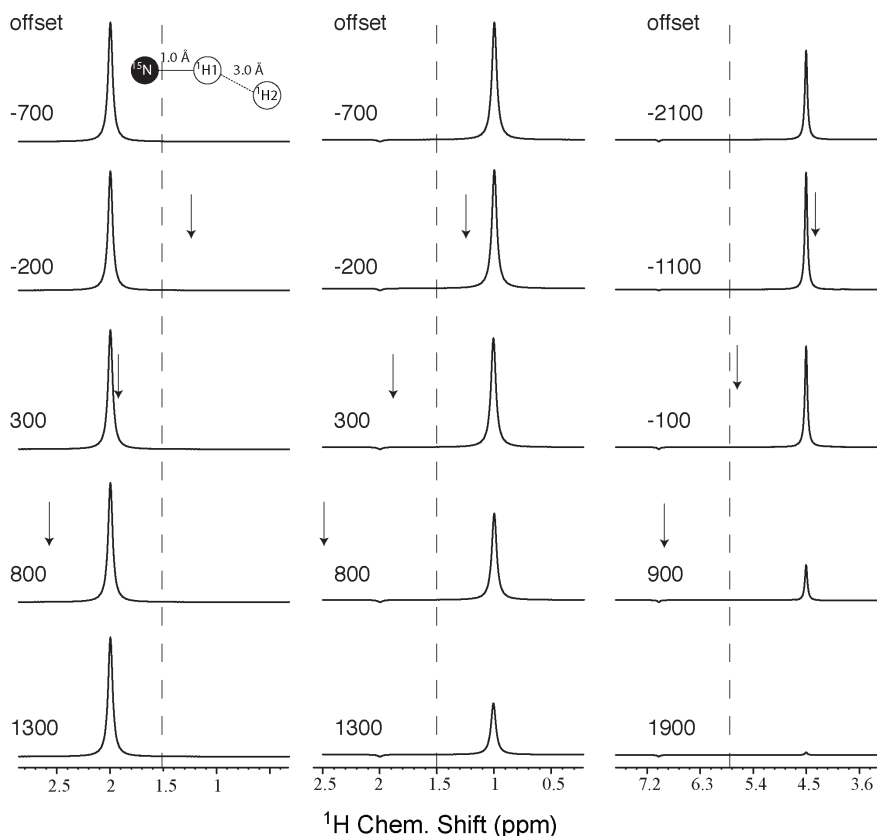
Figure S4. SIMPSON simulations of offset dependencies of HH CP (left) and iSOCP (middle and right) processes. The spin system used for the simulation is shown on the top and the input program is given in the previous section. For left and middle spectra, H_1 and H_2 protons have a chemical shift of 2 and 1 ppm, whereas for the right spectra, a chemical shift 4.5 and 7 ppm was considered. The offset values (i. e. relative carrier frequencies) depicted are related to the center of the two peaks (1.5 ppm for the left and middle column, 5.75 ppm for the right column) and are shown by arrows in case they are within the drawing area. The consistent predominant transfer from N to the lateral proton rather than the directly coupled proton is caused even in the absence of a respective heteronuclear dipolar coupling owing to a dipolar coupling between H_1 and H_2. In the simulations, the overall efficiency of the transfer decreases much faster for situations in which the carrier is increasingly off-resonance than in the HH CP cases. This is due to the square pulse instead of a ramp, whereas the strength (bandwidth) of the proton spin lock is very similar in both cases.

In comparison to the simulations, the offset of the iSOCP pulse in the real experiment seems to have a significantly smaller effect. There the offset was set to the water frequency in all NMR experiments, and the iSOCP is effective for the ^{13}C-edited as well as for ^{15}N-edited experiments and irrespectively of whether H_1 and H_2 are aliphatic or amide protons (see Main Text Figure 2 C and D). A lower offset sensitivity in the experiment than in the 3-spin simulation might be due to the residual dipolar-coupling network in the protein (multi-spin system), in which multiple protons with different chemical shifts will always be present in close proximity to the spin triple under consideration. Hence, the chance for all dipolar-connected protons being far off-resonance is low. Additionally, the selectivity to a small bandwidth of the perfect square pulse assumed in the simulation will be decreased by rf inhomogeneity in the real experiment.
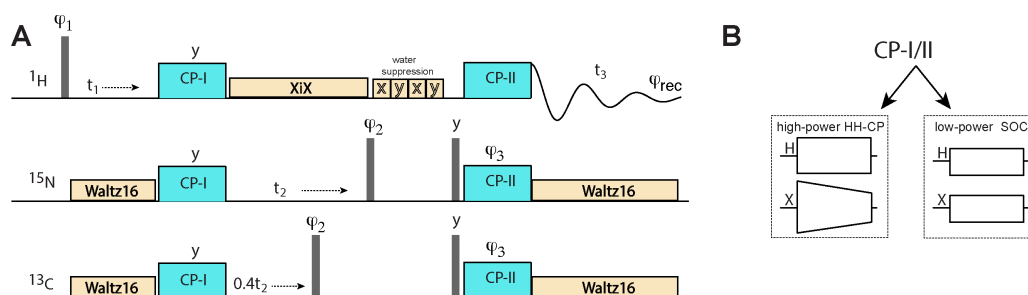
Figure S5. General pulse sequence for a time-shared ^{1}H-^{15}N/^{13}C-^{1}H-correlation experiment with (B) two cross polarization transfers (CP-I and CP-II). The cross polarization transfer step is either conventional Hartmann-Hahn CP transfer (ramped) or low-power SOCP transfer (see details above). All phases are x unless denoted otherwise. Two-step phase cycles were employed for ϕ_1, ϕ_2, and ϕ_3 upon according inversion of the receiver phase. Additionally, ϕ_2 was cycled in terms of TPPI phase-sensitive incrementation.

To assess the SIMPSON simulations experimentally, we performed ^{15}N-filtered 2D proton-proton correlation experiments (Figure S6). The basic pulse sequence used for recording these spectra (as well as for the 3D spectra described below) is shown in Figure S5. For CP-I and CP-II, we used either Double-Quantum Hartmann Hahn Cross Polarization (DQ-HH CP) or SOCP, resulting in four possible scenarios. Figure S6 C and D show the spectra obtained when either CP-I or CP-II is exerted as an SOCP and the other one as a DQ-HH CP, respectively. Indeed, the amide ^{15}N magnetization is now transferred predominantly from or to relayed aliphatic protons. Using either conventional or SOCP, a selective transfer between the heteronucleus and either a directly bonded ([1]H_1-type) or a relayed ([1]H_2-type) proton is elicited. Amide protons (according to [1]H_1 above) "see" aliphatic protons ([1]H_2) as strong lateral ^{1}H partners. This enables a directed transfer to the relayed proton [1]H_2 only, mostly excluding the directly bonded proton, which provides a plethora of new spectroscopic possibilities. For all these experiments, the proton offset was set to the water frequency.
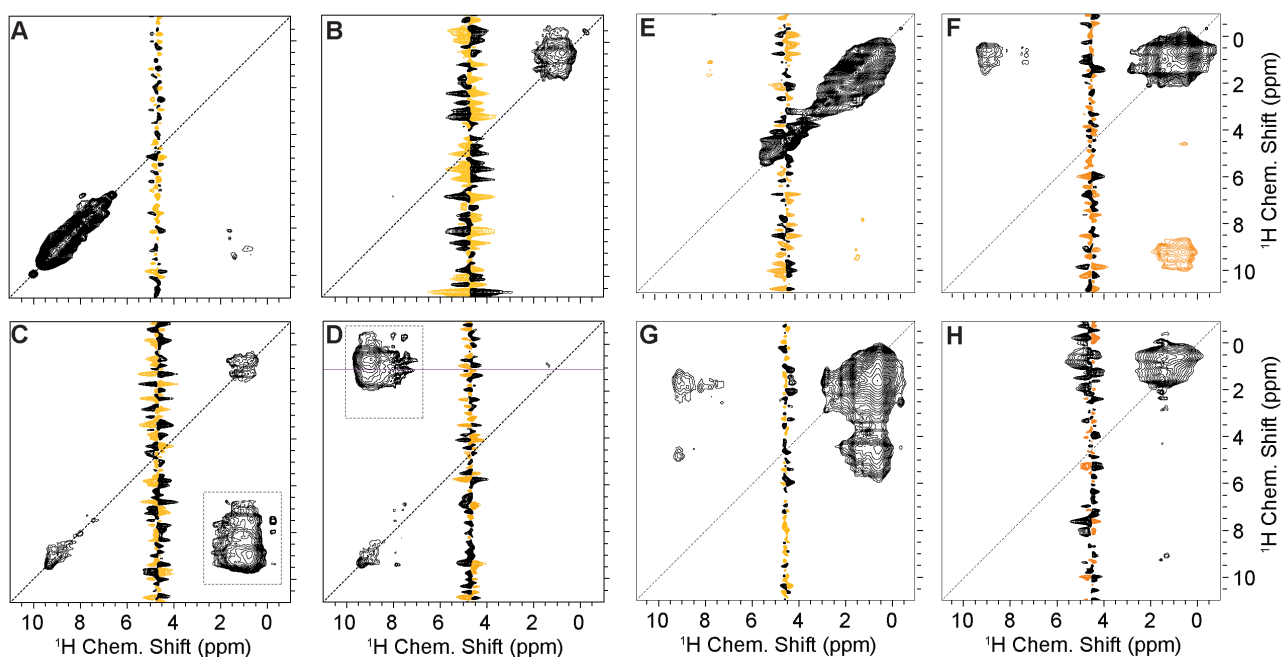
Figure S6. (A) – (D) 2D-X-filtered proton-proton correlation experiments employing the four different combinations for first and second CP steps in the pulse sequence shown in Figure S5, but using ^{15}N as a single heteronuclear channel only: (A) DQ HHCP – DQ HHCP, (B) SOCP – iSOCP, (C) DQ HHCP – iSOCP, (D) SOCP – DQ HHCP. (E) – (H): The ^{13}C-filtered complement of the proton-proton correlation experiments with the four combinations for first (CP-I) and second CP (CP-II) steps. (E) DQ HHCP – DQ HHCP, (F) SOCP – iSOCP, (G) DQ HHCP – iSOCP, (H) SOCP – DQ HHCP. The diagonal region is represented by dotted lines in the spectra. The non-time shared version (only the upper two lines of the pulse scheme) was used here, and heteronuclear evolution t_2 was omitted here for better clarity in a 2D experiment. All carrier frequencies (in the proton dimensions) were set to the water resonance.
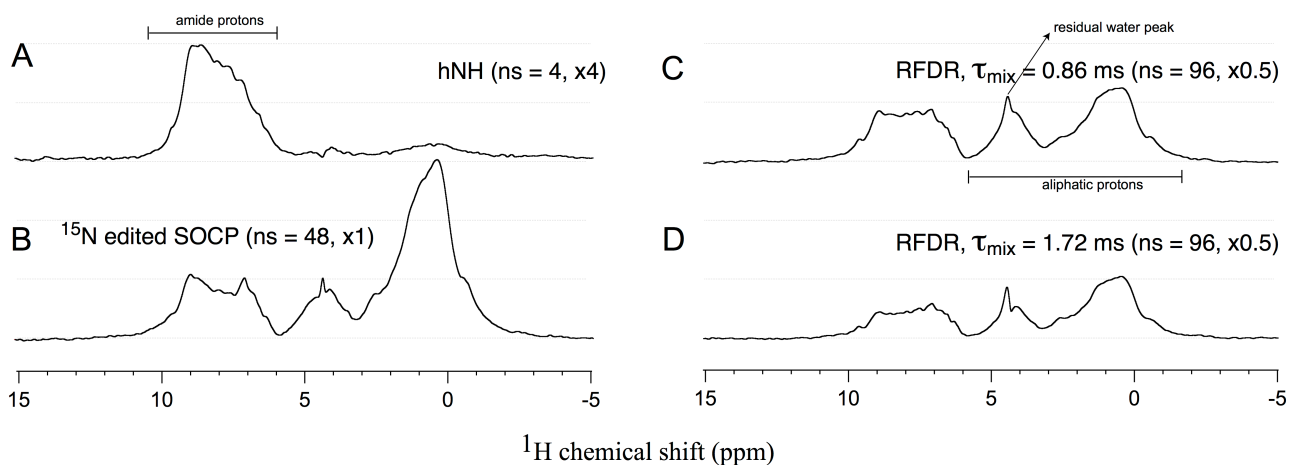
Figure S7. A sensitivity comparison of first-FID slices of the iSOCP approach (recorded here as a non-time-shared version) with 3D-RFDR homonuclear mixing for obtaining aliphatic proton information under similar experimental conditions. For all experiments in B–D the signal is scaled (the scaling factor is given in the parenthesis) to a total 48 scans. For all the spectra similar processing parameters were used. Here, first-FID slices of (A) 2D-hNH 2D, (B) ^{15}N-edited 2D-hNH with iSOCP, (C and D) 3D HNhH-RFDR with different mixing times are shown. The signals of interest are the aliphatic bulk in B, C, and D (transfer pathway according to $H^N \rightarrow N \rightarrow H^{ali}$). Simultaneous optimization of $H \rightarrow N/N \rightarrow H$ and $H \rightarrow C/C \rightarrow H$ CP/SOCP in the time-shared iSOCP experiment (main text) reduces the eventual sensitivity by approximately 20%. The RFDR experiment is weaker by more than a factor of two compared with iSOCP.
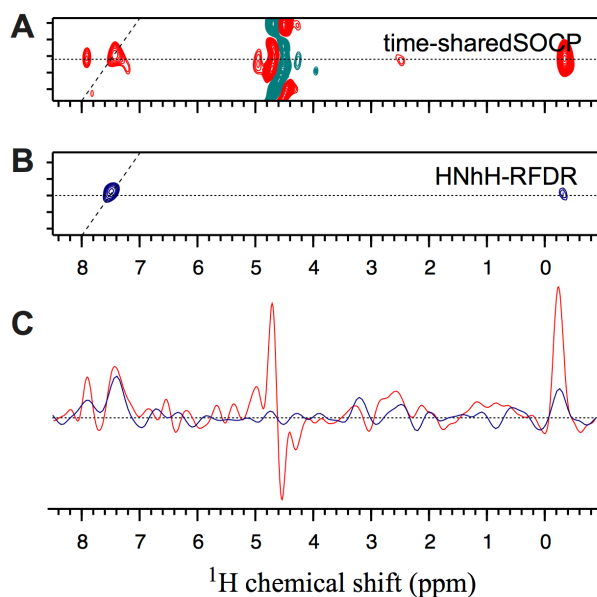
Figure S8. 3D stip plot comparison of the time-shared version of the iSOCP (A) approach with RFDR (B) homonuclear mixing. 1D cross sections of the strips along the proton dimensions (similar color coding as in A and B) are shown in (C). Similar processing parameters were used for the comparison and the total acquisition times are restricted to 5 ms for proton dimensions (both direct and indirect dimensions) and 12.3 ms for the nitrogen dimension. In contrast to the homonuclear mixing sequence RFDR, the magnetization is mostly directed to the lateral proton instead of the directly bounded one for iSOCP.

Diagonal peak proton	Observed unambiguous peaks	Observed ambiguous peaks	Unobserved peaks
8LH$_N$	8LH$_\beta$(2.53 Å)	---	7EH$_\alpha$(2.07 Å), 8LH$_\gamma$(2.67 Å)
9VH$_N$	9VH$_{\gamma2}$(2.29 Å)	---	8LH$_\alpha$(2.30 Å)
11AH$_N$	11AH$_\beta$(2.44 Å)	---	10LH$_\alpha$(2.09 Å), 10LH$_\delta$(2.41 Å)
12LH$_N$	12LH$_\beta$(2.48 Å)	12LH$_\gamma$(2.44 Å)	11AH$_\alpha$(2.07 Å), 13YH$_N$(2.4 Å)
13YH$_N$	12LH$_\beta$(3.01 Å)	---	---
16QH$_N$	16QH$_{\beta1}$(2.42 Å), 16QH$_{\beta2}$(2.92Å)	---	15YH$_\alpha$(2.22 Å)
19SH$_N$	22EH$_\beta$(2.39 Å)	---	18KH$_N$(1.88 Å)
23VH$_N$	23VH$_\gamma$(2.31 Å)	---	22EH$_\alpha$(2.28 Å), 22EH$_\beta$(2.51 Å)
24TH$_N$	24TH$_\beta$(2.59 Å), 24TH$_\gamma$(3.72 Å)*, 23VH$_{\gamma2}$(2.81 Å)	----	23VH$_\alpha$(2.37 Å)
24TH$_\alpha$	24TH$_\gamma$(2.84 Å)	---	---
24TH$_\beta$	24TH$_\gamma$(2.10 Å)	---	24TH$_N$(2.59 Å)
25MH$_N$	24TH$_\gamma$(2.87 Å)	---	24TH$_\alpha$(2.29 Å), 25MH$_\gamma$(2.4 Å)
26KH$_N$	---	26KH$_\beta$(2.52 Å)/ 26KH$_\gamma$(2.9 Å)	25MH$_\alpha$(2.25 Å), 25MH$_\beta$(2.53 Å)
27KH$_N$	27KH$_\beta$(2.67 Å)	---	26KH$_\alpha$(2.30 Å), 27KH$_\alpha$(2.58 Å)
28GH$_N$	11AH$_\beta$(2.64 Å)	27KH$_\gamma$(2.95 Å)	28GH$_\alpha$(2.32 Å), 27KH$_\alpha$(2.44 Å)
29DH$_N$	11AH$_\beta$(2.42 Å)	---	29DH$_\beta$(2.34 Å)
32TH$_\beta$	32TH$_\gamma$(2.28 Å)	---	32TH$_N$(2.53 Å)
31LH$_N$	---	31LH$_\gamma$(2.39 Å)	30IH$_\alpha$(2.21 Å), 31LH$_\beta$(2.67 Å)
33LH$_N$	33LH$_{\beta1}$(2.43 Å), 33LH$_{\beta2}$(2.63 Å)	---	32TH$_\alpha$(2.17 Å)
37TH$_N$	37TH$_\gamma$(2.27 Å), 36SH$_N$(2.59 Å)	37TH$_\alpha$(2.82 Å)/36SH$_\alpha$(3.01 Å)	---
37TH$_\alpha$	37TH$_\gamma$(2.56 Å)	----	37TH$_\beta$(2.45 Å)
37TH$_\beta$	37TH$_\gamma$(2.31 Å)	---	37TH$_\alpha$(2.45 Å)
39KH$_N$	40DH$_N$(2.61 Å), 39KH$_\alpha$(3.04 Å)*	39KH$_\gamma$(2.44 Å)/ 39KH$_\beta$(2.56 Å),	38QH$_\alpha$(2.26 Å), 41WH$_N$(2.24 Å)
39KH$_\alpha$	39KH$_N$(3.04 Å), 39KH$_\beta$(2.18 Å), 39KH$_\gamma$(3.2 Å), 42WH$_\epsilon$ (3.13 Å)	---	---
40DH$_N$	39KH$_N$(2.61 Å)/ 41WH$_N$(2.24 Å), 40DH$_\alpha$(2.89 Å)	---	40DH$_\beta$(2.38 Å)
41WH$_N$	40DH$_N$(2.24 Å)	--	41WH$_\beta$(2.59 Å)
41WH$_\epsilon$	41WH$_\delta$(2.54 Å), 41WH$_\zeta$(2.81 Å)	---	---
42WH$_\epsilon$	42WH$_\delta$(2.54 Å), 42WH$_\zeta$(2.80 Å), 55AH$_\beta$(3.38 Å)*, 39KH$_\alpha$ (3.13 Å)*	---	---
44VH$_N$	51GH$_N$(2.8 Å), 44VH$_\gamma$(2.21 Å)	33KH$_\gamma$(3.16 Å)*	43KH$_\alpha$(2.13 Å)
46VH$_N$	49RH$_N$(3.02 Å),	46V$_\gamma$(2.65 Å)	45Q$_\alpha$(2.15 Å)

49RH$_N$	49RH$_\beta$(2.51 Å)	---	48DH$_N$(2.39 Å)
49RH$_\delta$	49RH$_\epsilon$ (2.57 Å), 49RH$_\gamma$(2.34 Å)	---	---
50QH$_N$	50QH$_{\beta1}$(2.59 Å), 50QH$_\gamma$(2.85 Å)	---	49R$_\alpha$(2.26 Å)
51GH$_N$	---	23VH$_\beta$(3.69 Å)*, 23VH$_\gamma$(3.67 Å)* 44VH$_\gamma$(3.83 Å)*	---
55AH$_N$	56AH$_N$(2.82), 55AH$_\beta$(2.50), 55AH$_\alpha$(2.75)	---	54PH$_\alpha$(2.29 Å)
56AH$_N$	55AH$_N$(2.82), 57YH$_N$(2.68), 55AH$_\beta$(2.92), 56AH$_\beta$(2.57), 56AH$_\alpha$ (2.88)	---	---
57YH$_N$	56AH$_N$(2.68 Å),	58VH$_N$(2.50 Å)	57YH$_\beta$(2.45 Å)
58VH$_N$	---	58VH$_{\gamma1}$(2.99 Å), 58VH$_{\gamma2}$(2.35 Å), 57YH$_N$(2.50 Å)	---
60KH$_N$	---	60KH$_\beta$(2.28 Å)/ 60KH$_{\gamma2}$(2.71 Å)	59KH$_\alpha$(2.45 Å)
61LH$_N$	---	61LH$_\beta$(2.57 Å)	60KH$_\alpha$(2.28 Å)

Table S1. The experimentally observed cross-peaks (lateral protons), their corresponding distances to their amide proton as obtained from the X-ray crystal structure, PDB 2NUZ. In the fourth column, all other protons are listed that do not appear even though they are within a range of 2.75 Å. Most of these cases represent H$_\alpha$ correlations in which peak positions coincide with the water peaks and cannot be extracted. Peaks with an asterisk denote observed cross-peaks with distances above a 3 Å limit. In some cases, one of the beta/gamma proton distances from the amide proton is shorter than the other one. For simplicity, the shorter distance is only mentioned here.
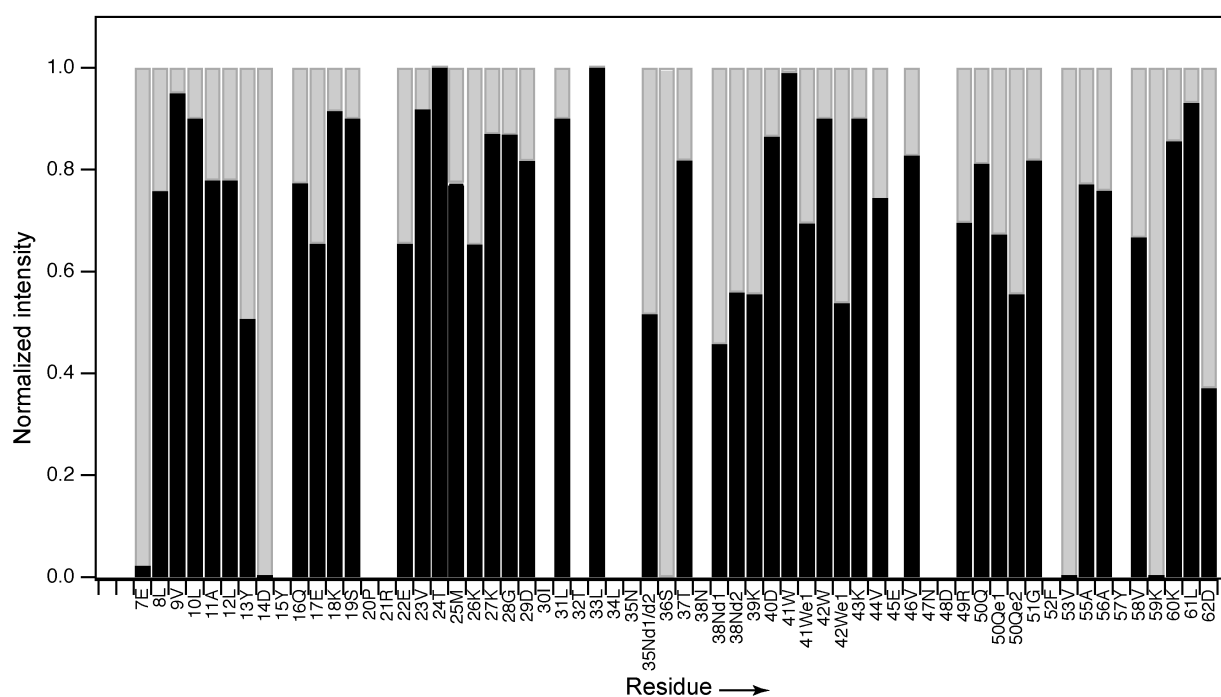
Figure S9. Normalized intensities of diagonal (grey color) and cross-peaks (black color) of amide proton resonances in a 3D ^{1}H-^{15}N-^{1}H-correlation experiment (Figure 3). The intensities are calculated from the integrations of 1D slices (along the direct dimension). For normalization the sum of the diagonal and cross-peak intensities are set to unity. For side chain protons as a diagonal signal (H$_\delta$ of Asn and H$_\varepsilon$ of Gln), the ratio is close to 0.5, resembling the XH$_2$ spin system simulation as shown in Figure S3D and S3F. Those amide protons for which cross-peaks are not observed and those for which the amide diagonal peaks are not resolved result in gaps. For unresolved strips, the ratio was calculated together and the value is listed for both residues.
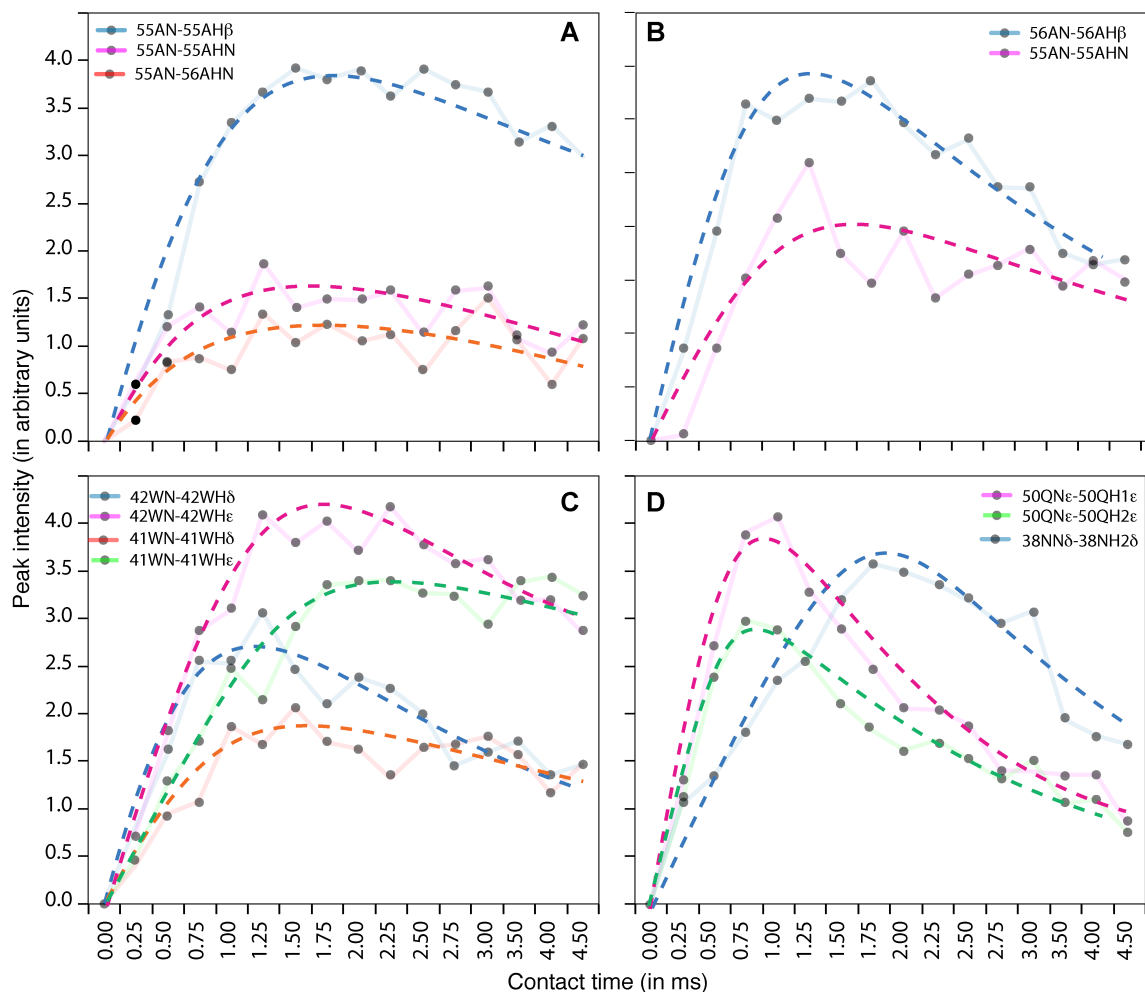
Figure S10. Build-up curves of both diagonal- and cross-peaks with the variation of iSOCP contact time for various residues resolved in 2D ^{1}H-^{15}N correlations: (A) 56Ala, (B) 55Ala, (C) 41Trp and 42Trp side chain, and (D) 50Gln and 38Asn. All buildup maxima are obtained using a contact time on the order of 1-2 ms. All buildups were measured with a ^{15}N-edited 2D version of the sequence mentioned as above and as depicted in Figure S5 with the first and second CPs being HHCP and iSOCP, respectively. All other experimental parameters were kept similar as described above. Experimental errors for each point amount to approximately 0.3 a. u., if purely derived from the noise of the data sets. Trendlines assume mono-exponential decay functions for buildup and decay. All proton pairs shown here have a distance between 2 and 2.4 Å.
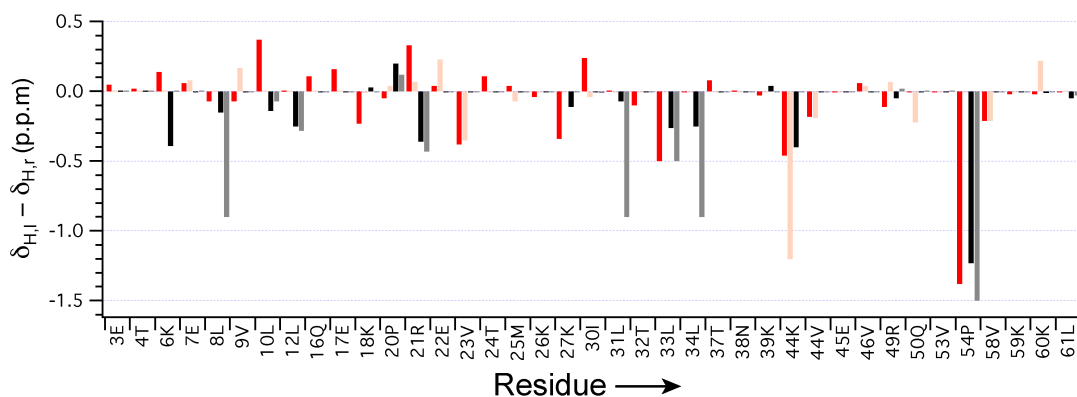
Figure S11. Deviations of SH3 Hγ and Hδ (Hγ: red, light red, Hδ: black, grey color) proton chemical shift (as reported earlier by van Rossum et al.[5]) from random coil shifts[6] as a general property reporting on the local spin environment.

Residue	Hα	Hβ	Hγ/others
8Leu	5.06(4.38)	0.85(1.65)	---
10Leu	5.00(4.38)	---	H$_\delta$:0.62 (0.9)
11Ala	4.26(4.35)	1.44(1.39)	---
12Leu	3.66(4.38)	0.57(1.65)	---
13Tyr	4.30(3.13)	2.95(2.92)	---
16Gln	4.17(4.37)	1.61(2.07), 2.10(2.07)	---
22Glu	---	1.59 (2.09)	---
23Val	4.31(4.18)	1.60(2.13)	0.41(0.96)
24Thr	5.30(4.35)	3.67(4.22)	1.2(1.23)
25Met	4.68(4.52)	2.05(2.08)	---
26Lys	4.42(4.36)	1.30(1.80)	---
27Lys	3.25(4.36)	1.39(1.80)	---
29Asp	4.56(4.76)	2.24(3.88)	---
31Leu	---	0.77(1.65)	---
32Thr	4.34(4.35)	---	1.08(1.23)
33Leu	---	1.1(1.65), 0.44(1.65)	---
36Ser	3.89(4.5)	2.44(3.88)	---
37Thr	3.89(4.35)	4.3(4.22)	1.33(1.23)
39Lys	4.06(4.36)	1.74(1.80)	1.32(1.45)
40Asp	4.14(4.76)	1.81(3.88)	---
41Trp	---	---	H$_\delta$:7.06(7.24),H$_\zeta$:7.4(7.5)
42Trp	---	---	H$_\delta$:7.2(7.24),H$_\zeta$:7.5(7.5)
43Lys	4.67(4.36)	1.05(1.80)	0.85(1.45)
44Val	5.04(4.18)	1.77(2.13)	0.5(0.96)
46Val	4.32(4.18)	1.69(2.13)	---
49Arg	---	1.69(1.84)	1.75(1.70), H$_\delta$:3.3(3.32)
50Gln	5.33(4.37)	1.57(2.07)	1.8(2.38)
51Gly	3.96(3.97)	---	---
53Val	4.63(4.18)	1.47(2.13)	0.81(0.96)
55Ala	2.62(4.35)	-0.38(1.39)	---
56Ala	3.83(4.35)	1.05(1.39)	---
58Val	5.17(4.18)	1.61(2.13)	0.61(0.96)
59Lys	4.63(4.36)	1.43(1.80)	---
60Lys	4.10(4.36)	1.56(1.80)	---
61Leu	4.15(4.38)	1.51(1.65)	---
62Asp	4.12(4.76)	2.45(3.88)	---

Table S2. Experimentally observed aliphatic proton chemical shifts in the SH3 domain in the solid-state at a sample temperature of 35 °C. In parentheses, random-coil chemical shifts are given for comparison.

References:

(1)   Linser, R.; Chevelkov, V.; Diehl, A.; Reif, B. *J. Magn. Reson.* **2007**, *189*, 209.
(2)   Zhou, D. H.; Rienstra, C. M. *Journal of Magnetic Resonance* **2008**, *192*, 167.
(3)   Linser, R.; Bardiaux, B.; Higman, V.; Fink, U.; Reif, B. *J. Am. Chem. Soc.* **2011**, *133*, 5905.
(4)   Bak, M.; Rasmussen, J. T.; Nielsen, N. C. *Journal of Magnetic Resonance* **2000**, *147*, 296.
(5)   van Rossum, B.-J.; Castellani, F.; Rehbein, K.; Pauli, J.; Oschkinat, H. *ChemBioChem* **2001**, *2*, 906.
(6)   Wishart, D. S.; Bigam, C. G.; Holm, A.; Hodges, R. S.; Sykes, B. D. *J. Biomol. NMR* **1995**, *5*, 67.